High Specific-Impulse Electrospray Explorer Trajectory Guidance and Control Air Bearing Demonstration

Michael Moncton*
NASA Jet Propulsion Laboratory, California Institute of Technology, La Cañada Flintridge, California 91011

Oliver Jia-Richards†
Massachusetts Institute of Technology, Cambridge, Massachusetts 02139

David Sternberg‡, Kevin Lo§, and Swati Mohan¶
NASA Jet Propulsion Laboratory, California Institute of Technology, La Cañada Flintridge, California 91011

As small satellite mission concepts that require travel further from their traditional domain of low-Earth orbit are being considered, there is a growing need to develop small scale propulsion systems that can provide the necessary net impulse to enable deep-space operation. The High Specific-impulse Electrospray Explorer for Deep-Space (HiSPEED) project is an example concept considered for this paper, since it would be a small satellite that uses electrospray thrusters to navigate along a low-thrust spiral trajectory from Earth to a near-Earth asteroid. The NASA Jet Propulsion Laboratory Small Satellite Dynamics Testbed operates simulation and air bearing testing environments. This paper focuses on its planar air bearing platform used to create a nearly frictionless environment in three degrees of freedom: two translational and one rotational. The platform maneuvers using eight compressed air thrusters controlled by an onboard single board computer using position feedback from a motion capture system. This paper discusses the design, development, and testing of a closed-loop controller for this platform that enables trajectory following with position error less than four centimeters. The paper presents data from tests representative of HiSPEED spiral escape trajectories and operations in proximity to an asteroid along with implications for HiSPEED and similar concepts.

Nomenclature

a_p	=	propulsive acceleration, m/s^2
f	=	cost function
i	=	time index
j	=	waypoint index
n	=	linear programming sample point
r	=	radius, m
r_0	=	initial radius, m
t	=	time, s
t_{esc}	=	escape time, s
T	=	total trajectory time, s
$u_{\max}$	=	maximum control input, m/s^2
u_x	=	control along x-axis, m/s^2
u_y	=	control along y-axis, m/s^2
v_0	=	initial orbital speed, m/s
v_x	=	velocity along x-axis, m/s

*Currently Ph.D. Candidate, Department of Aerospace Engineering Sciences, University of Colorado Boulder
†Currently Assistant Professor, Department of Aerospace Engineering, University of Michigan, oliverjr@umich.edu, AIAA Member.
‡Guidance and Control Engineer, Section 343, david.c.sternberg@jpl.nasa.gov, AIAA Member
§Guidance and Control Engineer, Section 343
¶Guidance and Control Engineer, Section 343, AIAA Member

v_y = velocity along y-axis, m/s
W = waypoint
x = x-axis position, m
y = y-axis position, m
γ = ratio of propulsive to gravitational acceleration
δ = waypoint stop flag
Δt = control time step, s
μ = gravitational parameter, m^3/s^2
τ = waypoint time step, s

I. Introduction

There has been a growing interest in using CubeSat spacecraft (those with a characteristic dimension of 10 cm [1]) and other small satellite form factors for missions traveling beyond Earth's orbit, especially those with technology maturation and scientific goals. For example, the Mars Cube One (MarCO) CubeSats were the first to travel to another planet, serving as a communications relay system while demonstrating new technologies for deep space operation of CubeSats. Additionally, Lunar Flashlight had been launched to conduct a scientific exploration for water ice in permanently-shadowed craters of the Lunar South Pole. Missions traveling beyond Earth orbit require that the spacecraft have the capability of managing momentum, pointing the spacecraft, and adjusting its cruise trajectory. Those missions that orbit other bodies also need to enter and maintain the desired orbits. These mission requirements can be met by using thrusters, which provide forces and torques for translation and rotation of the spacecraft.

Thrusters on deep-space CubeSats and small satellites have traditionally been chemical, rather than electric, owing to the limited lifetime of existing CubeSat-scale electric propulsion systems; the emitters of many electrospray thrusters wear down over time, limiting their effective firing durations. For this reason, MarCO [2] used a VACCO biphase propellant system, and Lunar Flashlight [3] used a green monopropellant system. However, the ability to use electric propulsion would enable small spacecraft to perform more demanding missions, such as propelling themselves to their own targets. To circumvent the problem of low firing times for CubeSat electric propulsion systems, one proposed solution is to discard spent thrusters through staging, analogous to launch vehicles staging spent boosters. Staging of electrospray thrusters was originally proposed in order to reduce the overall time of Lunar missions by enabling longer net firing times across all stages [4].

The High Specific-impulse Electrospray Explorer for Deep-Space (HiSPEED) concept [5], jointly developed by the Massachusetts Institute of Technology (MIT) and the NASA Jet Propulsion Laboratory (JPL), is a technology maturation project to further develop staging systems for electrospray thrusters in order to enable a CubeSat mission to a near-Earth asteroid. The required mechanisms to enable a staging system were designed [6] and tested in a vacuum environment [7] providing confidence in the feasibility of using a stage-based electrospray propulsion system for an asteroid to a near-Earth asteroid. Therefore, HiSPEED will use stages comprised of electrospray thrusters and their corresponding fuel tanks until the thrusters reach their operational lifetime limit. Once the thrusters reach their lifetime limit, the complete stage is ejected from the rest of the spacecraft using a small spring actuator, revealing the next stage and its fresh thrusters in order to continue the mission. Fig. 1 shows a conceptual image of staging with an array of electrospray thrusters on a 3U CubeSat.

Characterizing the behavior of subsystems is necessary to build confidence in spacecraft flight performance predictions. Many smaller missions, however, do not have the financial or temporal means with which to conduct a testing campaign as thorough as larger-scale missions. As a result, requirement verification and validation steps are often reduced. One way of mitigating this risk is to utilize a dedicated testbed that can be shared across multiple missions, thereby amortizing the cost of the testbed across many projects to decrease the costs for each.

The Small Satellite Dynamics Testbed (SSDT) is a guidance and control laboratory founded at JPL in 2014 designed originally to test attitude control systems on small satellites under 30 kg in mass, including CubeSats. The testbed has three platforms with which hardware can be characterized: a spherical air bearing platform, a planar air bearing platform, and a robust simulation environment [8]. The spherical air bearing testbed, allowing rotation in three degrees of freedom, can be used to test entire spacecraft attitude control subsystems or individual components to characterize their dynamics, while the planar air bearing testbed, with one rotational and two translational degrees of freedom allows for testing of spacecraft components like accelerometers and inertial measurement units. The planar air bearings operate either in the SSDT or in the JPL Formation Control Testbed (FCT), which has a large flat floor for performing translation-dependent

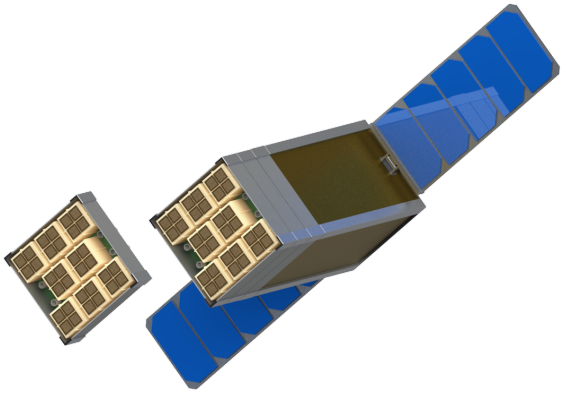

Fig. 1 HiSPEED concept image, showing a staging event.

testing. The SSDT also maintains a library of components with thoroughly modeled and understood characteristics for use on either the planar or spherical air bearings; models of the hardware are also included in the simulation. The simulation environment, created in MATLAB and Simulink, can not only model the performance of both air bearing systems, including friction and environmental effects, but also extrapolate the results of tests done on the two air bearing platforms to performance in orbit including effects such as atmospheric drag, solar radiation pressure and torque, and local magnetic field. As a result, the simulation is useful for obtaining performance estimates for ground tests and for in-flight operations.

This paper describes the development of a thruster system for the SSDT planar air bearing robotic platform with HiSPEED as a concept mission. In doing so, the paper provides a technical summary of the implemented system as well as a contribution to the field through the capture of performance metrics, an assessment of error sources, and options for follow-on development to support missions like HiSPEED. First, the paper presents an overview of the state of the SSDT planar air bearing system prior to the developments made to test the HiSPEED analog, followed by the development process of the spacecraft trajectory generator and thruster controller. Additionally, the paper presents a test campaign to mature the HiSPEED controller, including a selection of results that demonstrate the effectiveness of the SSDT thrusting planar air bearing at acquiring performance characteristics of a low-thrust CubeSat. Finally, future improvements are discussed that will further the ability of the SSDT to help mature the HiSPEED controller to flight-readiness.

II. Small Satellite Dynamics Testbed Thrusting Planar Platform

A. Planar Air Bearing Capabilities

The primary purpose of developing planar air bearing platforms is maturing and testing guidance, navigation, and control hardware and software. Air bearing platforms can accomplish this in multiple ways, including testing individual components, fully integrated attitude control systems, or even entire small sized satellites. Notably, the work in this paper lays the foundation for subsequent development of flight hardware and software. First, however, the testbed needs to be developed and understood to the point where results obtained from using the testbed can be deemed sufficient to meet the needs of the project. This paper focuses on that initial testbed development phase. If scaled properly, entire trajectories can be simulated on the FCT flat floor, allowing the testing of controllers throughout the entire range of expected operations. Detailed proximity operations can be performed, testing various aspects of control systems such as vision systems under varying conditions and direct sampling of target bodies.

The SSDT maintains a library of flight attitude control system hardware that enables various users of the testbed to perform subsystem-level testing by selecting the relevant actuators and sensors for their mission scenario. Though the hardware library includes integrated systems, reaction wheels, inertial measurement units, and star trackers, it is impractical to maintain a set of thrusters in the hardware library. Flight thruster systems have large variation across missions, potentially hazardous propellants, potentially restricted operation in vacuum only, and have a limited consumable in its propellant. Consequently, the SSDT has developed a compressed air thruster system for use on the planar air bearing that can be controlled using pulse-width modulation to produce net forces and torques akin to those

produced by flight systems, including those that cannot be tested in the ground environment, such as electrosprays. Electrospray thrusters, like those planned for a HiSPEED flight mission can only be operated in vacuum, so the pulse-width modulated compressed air thrusters provides an analog for the thrust performance expected in flight. This SSDT propulsion system is therefore a ground analog to the flight systems to enable the testing of critical aspects of the attitude control and propulsion control systems.

If they are small enough, fully assembled satellites can be tested as well. Designed to carry payloads as large as 30 kg, the test platform can easily support all sizes of CubeSat and small ESPA-class satellites. Testing the attitude control on a fully completed satellite is an excellent way to confirm the functionality and performance of pointing controls, an essential part of any spacecraft's mission. The small scale of HiSPEED and similar satellites affords the advantage of making such testing possible, thereby significantly reducing mission risk. With the hardware fully integrated into the full satellite assembly, testing mock trajectories or proximity operations using both position and attitude thruster-based control with the flight-ready hardware setup is an excellent opportunity to debug flight systems and further characterize performance. As the platform can load scaled trajectories, the spacecraft can run through trajectories representative of what an actual orbital trajectory would look like when projected to a plane to determine how the controller would react to error from disturbances on the trajectory and what segments of the trajectory are prone to error.

Finally, the platform can be utilized for proximity operations. Currently, the platform can perform relative navigation, maneuvering relative to another object tracked by the Vicon system, consisting of 10 cameras mounted around the walls of the FCT facility. The system is used to track the position and orientation of the objects on the FCT floor as either a truth sensor or as a way to provide data to a spacecraft's state estimator. Once vision systems that currently are in development have been incorporated, the platform can provide a means of testing proximity operations, from visual target tracking to maneuvering relative to the target object. As the FCT has a large spotlight to simulate the sun, vision systems can be stressed in a multitude of lighting conditions while maneuvering relative to other objects on the floor. FCT also has a large- comet surface simulation currently installed on one side of the floor, which provides realistic surface features.

B. Thruster System for Planar Air Bearing

The SSDT planar air bearing test platform is a compressed air system that runs off of two internal tanks of atmospheric air compressed to a maximum of 2400 psi. The two air tanks feed both the three air bearings that allow the platform to float and the eight thrusters that allow it to maneuver, with regulators limiting the pressure to the bearings and the thrusters to 90 psi. Compressed air is fed through holes in the bottoms of the air bearings, creating a thin layer of air between the bearings and the floor. Without direct surface to surface contact, the platform can move in a nearly frictionless environment that mimics how a satellite might move in free space. Also operating at 90 psi, the thrusters are mounted on the bottom plate of the platform and are oriented with two pointing in each cardinal direction. Fig. 2 shows the thruster numbering conventions used by the control algorithm, as well as a definition of the coordinate systems in the platform (body-fixed) and lab (inertial) frames of reference. In the figure, the arrows emanating from the platform represent thruster exhaust directions.

An Atlas Single Board Computer connected to an Emerald-MM-8PLUS 8-Port Serial Module, both made by Diamond Systems and mounted on the test platform, controls the eight thrusters. The General Purpose Input/Output (GPIO) pins on the Atlas and Emerald boards control the solenoids responsible for opening and closing the thrusters, with the Emerald board responsible for opening the thrusters and the Atlas board responsible for closing the thrusters. Further details about the actuation of the thrusters is provided in [9].

Communications with the platform were accomplished using the local SSDT Wi-Fi network through a wireless USB network adapter connected to the Atlas board. Connected to this network were the test platform, a Vicon Motion Capture System, and a ground station computer running a Linux virtual machine. Used primarily to send initialization and test commands, the ground station also served as a convenient way to edit, compile, and upload new flight software via its virtual machine, which emulated the real time Linux environment on the platform. The platform received position data from the Vicon system. These cameras track six retroreflective objects mounted on the top or sides of the platform, in locations that would be most visible to the largest number of cameras. The Vicon system then created an object that represents the connected tracking objects and relays a packet containing the position, velocity, and heading of the platform over the Wi-Fi to the Atlas board, which utilizes the information for its position and attitude controllers.

It is important to note that air bearing platforms are commonly used to provide nearly frictionless surfaces for testing space dynamics in the constrained ground environment. A comparison of other planar air bearing testbeds is included within Ref. [9]. As noted in this comparison, the SSDT is distinguished by its emphasis on traceability

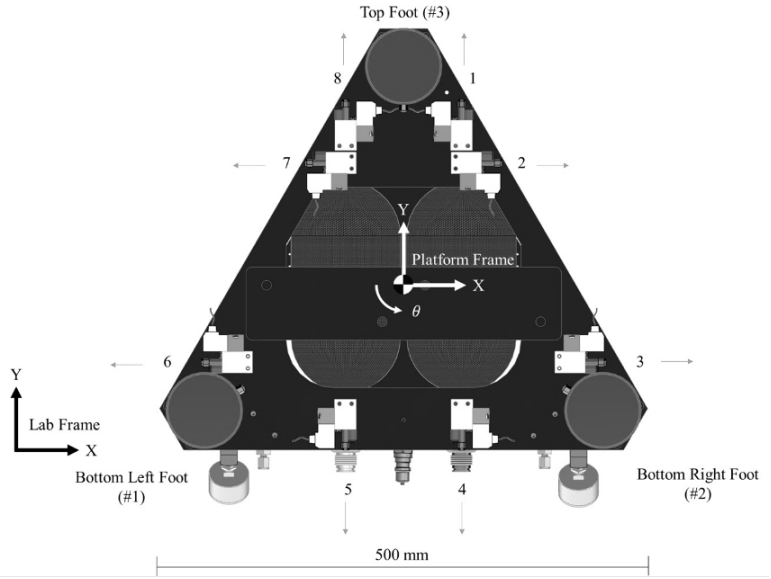

Fig. 2 Thruster arrangement of the planar air bearing platform.

to flight, its relatively sophisticated sensor suite and testing infrastructure for a small satellite testing system, and its inherent modularity, which enable it to support a wide variety of applications, from individual components or software algorithms to full flight vehicles. To support this diverse set of research and flight applications, compared to other testbeds, the SSDT planar air bearing has the highest payload capacity and per-thruster force of any planar platform in the survey besides ASTROS, a much larger platform. It therefore affords higher peak linear and angular accelerations that the platform can achieve.

C. SSDT Planar Air Bearings for HiSPEED Testing

The HiSPEED project is currently working closely with the SSDT. The HiSPEED mission utilizes staged electrospray thrusters mounted on a 6U CubeSat frame. By arranging thruster arrays in a staging configuration similar to that of a launch vehicle, with disposable stages, the mission would circumvent the limited lifespan of electrosprays to greatly increase the maximum burn time of the spacecraft, allowing exploration of deep space using a CubeSat framework. Using a similar form factor to that of the MarCO CubeSats, HiSPEED can generate 3500 m/s of Δv, far greater than MarCO's 30 m/s. Utilizing its high Δv capacity, HiSPEED's mission is to rendezvous with an asteroid escaping Earth's gravity under its own power. However, due to the low thrust nature of electrospray thrusters, a long escape spiral is necessary to leave Earth's gravity well. This escape trajectory was one of the first trajectories to be tested on the planar air bearing platform, and HiSPEED is to be the first project to utilize the test platform's enhanced operating capacity.

III. Trajectory Generator

The goal of the trajectory generator was to generate representative trajectories of the desired HiSPEED maneuvers that can be tested on the air bearing platform. As the trajectories are nearly 2D, the restriction to operating in a planar environment does not significantly affect the expected 3D performance. Two situations are considered: the low-thrust spiral of the HiSPEED spacecraft as it escapes from Earth and maneuvering of the spacecraft during proximity operations around the target asteroid. These scenarios are considered separately as they use distinct methods for generating trajectories. In both cases, trajectories need to be scaled, in time and space, to be completed within the capacity of the air bearing platform air tanks and to fit on the flat floor. These tests are key in demonstrating the control architecture and trajectory generation tools for a low-thrust propulsion system like that planned for HiSPEED. The staging dynamics, however, are not tested in this work, though follow-on testing is planned. For that future testing, a second planar air bearing will serve as a mock electrospray thruster stage.

Initial trajectories for the HiSPEED mission were generated under the assumption of constant thrust and take the

spacecraft from geostationary orbit to a rendezvous with asteroid 2010 UE51 [5]. Throughout the vast majority of the initial escape spiral, the spacecraft maintains a velocity-pointing control law. For the final legs of the escape spiral and the actual rendezvous with the asteroid, the trajectory is designed in order to minimize overall flight time. While the assumption of constant thrust will be invalid during the actual mission due to eclipses, the total eclipse time is small (10s of hours) relative to the total trajectory time (100s of days) and is not expected to significantly impact the final trajectory in either time or shape.

The HiSPEED trajectory results in maximum spacecraft-Earth distances on the order of 10^7 km. Scaling the full trajectory down to the size of the flat floor, order 1 m, means that the expected accuracy of the Vicon system, order 1 mm, equates to errors on the order of 104 km for the HiSPEED trajectory. This level of scaling would make it difficult to properly assess the expected performance of the HiSPEED spacecraft based on the performance of the air bearing platform. In particular, during the initial escape spiral the radial distance between revolutions of the spiral is less than 10.3 km meaning that the measurement noise from the Vicon system would span at least 10 revolutions of the spiral.

In order to resolve this issue, two steps are taken. First, only small segments of the trajectory are tested on the flat floor thereby lowering the necessary scaling. In doing so, the overall trajectory can be broken into multiple smaller pieces for lower overall errors. Second, alternative trajectories than the one generated for HiSPEED are used to represent the escape spiral. These alternative trajectories can be described analytically and allow the trajectory itself to be scaled by varying the gravitational parameter of the central body or the propulsive acceleration. This allows for trajectories that can represent full escape maneuvers, around planetary bodies other than Earth, while being appropriately scaled for testing on the flat floor. Since these trajectories are dynamically consistent, the equivalent trajectory for escape from Earth with an electrospray propulsion system can be generated and tested in simulation to compare expected performance to the observed performance on the air bearing platform. By breaking the complete trajectory into phases, the most pressing testing dynamics challenges can be addressed individually with unique mitigation steps.

For proximity operations, scaling presents less of an issue. The asteroid targeted in the initial HiSPEED trajectories, 2010 UE51, has an estimated diameter of approximately 10 m [10] allowing gravitational acceleration to be neglected and the spatial scaling to be less severe. Trajectories are designed to maneuver the spacecraft around the asteroid in order to emulate a potential visual survey of the asteroid's surface in 2D.

A. Low-Thrust Escape Trajectories

Low thrust trajectories have been used for decades to enable the robotic exploration of the solar system. These trajectories often have made use of other forms of electric propulsion to provide near-continuous low levels of thrust as compared to shorter chemical thrusting events. As a result of this difference in operation, low-thrust trajectories must be derived and controlled differently. While on a low-thrust trajectory, spacecraft must maintain pointing to enable the thrust direction to be controlled. The Dawn mission is one example of a low-thrust trajectory spacecraft, and its pointing constraints for determining optimal pointing quaternions using onboard vector tables and Chebyshev polynomials are described in [11], and the pointing accuracy for Dawn was presented in [12]. The software used to compute and analyze the Dawn trajectories, named Mystic, is described in [13]. Likewise, the mission design for the low-thrust mission Deep Space 1 is provided in [14]. These missions were significantly larger than HiSPEED, and their electric propulsion systems were of different types than the proposed HiSPEED electrospray thrusters that would benefit from a staged concept of operations. However, their approach to computing low-thrust trajectories is similar in that a reference position and attitude area always propagated and available for use by the onboard controllers. The implementation for HiSPEED does not use a scaled Chebyshev polynomial, however, as for HiSPEED an analytical trajectory model is developed for use with linear programming to reduce the need for creating parameterizations of the optimal solution.

The analytical form of the low-thrust escape trajectories is from an energy-based derivation. This trajectory has been modified and tested in simulation for guidance of a spacecraft between circular orbits with a staged propulsion system [15]. However, for the initial testing presented in this work, the effects of staging are not considered. In the analytical trajectory, the spacecraft is assumed to be in a near-circular orbit which allows the radial position of the spacecraft to be described as

$$r(t) = \frac{r_0}{\left(1 - \frac{a_p}{v_0} t\right)^2} \tag{1}$$

where r_0 is the initial orbital radius of the spacecraft, a_p is the magnitude of the propulsive acceleration, and v_0 is the initial orbital speed of the spacecraft. With this trajectroy, the time at which the spacecraft escapes the central body can

be estimated from

$$t_{\text{esc}} = \frac{v_0}{a_p}\left[1 - (2\gamma)^{1/4}\right] \tag{2}$$

where γ is the ratio of the propulsive acceleration to the gravitational acceleration at the start of the trajectory

$$\gamma = \frac{a_p}{\mu/r_0^2} \tag{3}$$

where μ is the gravitational parameter of the central body. Substituting the escape time into the Eq. 1 allows the radial position at escape to be written as

$$r(t_{\text{esc}}) = \frac{r_0}{(2\gamma)^{1/2}} \tag{4}$$

Therefore, for a given initial position on the flat floor, which sets r_0, a ratio of propulsive acceleration to gravitational acceleration can be picked in order to have the planar air bearing reach "escape" within the bounds of the flat floor. Furthermore, for a particular γ, the time scaling can also be set by choosing the appropriate propulsive acceleration. Under the circular orbit assumption, the initial orbital velocity of the spacecraft is

$$v_0 = \sqrt{\mu/r_0} \tag{5}$$

which allows the escape time to be written as

$$t_{\text{esc}} = \sqrt{\frac{r_0}{\gamma a_p}}\left[1 - (2\gamma)^{1/4}\right] \tag{6}$$

Alternatively, the escape time can be written in terms of the gravitational parameter of the central body as

$$t_{\text{esc}} = \frac{r_0^{3/2}}{\gamma\sqrt{\mu}}\left[1 - (2\gamma)^{1/4}\right] \tag{7}$$

It is worth noting that in both Eq. 6 and Eq. 7 the propulsive acceleration and gravitational parameter are that of the scaled system. With the scaling appropriately set, and the parameters r_0, a_p, and μ chosen, the trajectory can be designed as a set of individual waypoints for a single stage system. Each waypoint, W, can be described as

$$W[j] = \{x, y, \tau, \delta\} \tag{8}$$

where x, y is the waypoint's position, τ is the time the planar air bearing has to move from waypoint $j-1$ to waypoint j, and δ is a flag that indicates if the planar air bearing has to stop at the waypoint.

Figure 3 shows a comparison of a scaled trajectory used for testing on the flat floor and a potential escape trajectory for the HiSPEED mission. The flat-floor trajectory was generated with an initial radius of 0.4 m, a final radius of 1.5 m, and a total trajectory time of 120 seconds. The HiSPEED trajectory assumed that the spacecraft started in geostationary orbit and had a propulsive acceleration of 340 μm/s^2, the expected propulsive acceleration for the HiSPEED spacecraft. Both trajectories were designed based on the method in Ref. [15] for a single stage system. The flat-floor trajectory in essence is therefore a scaled representation of the final revolution of the HiSPEED spacecraft around Earth prior to escape, allowing for a simple method to generate trajectories for the flat floor that can capture the dynamics of an actual escape trajectory.

B. Proximity Maneuvering

Given the actuation setup of the air bearing platform, the position and attitude control can be decoupled; torque commands from an attitude controller are separately computed from force commands from the position controller. Therefore, the position dynamics can be written as a linear function of the input thrust along the x- and y-axes of the flat floor frame allowing linear programming to be used to design trajectories as in [16]. Trajectories are designed through a series of waypoints in order to minimize the overall control usage. Waypoints have a corresponding (x, y) position as well as a time, indicating the time allowed for the planar air bearing to move to the given waypoint from the previous

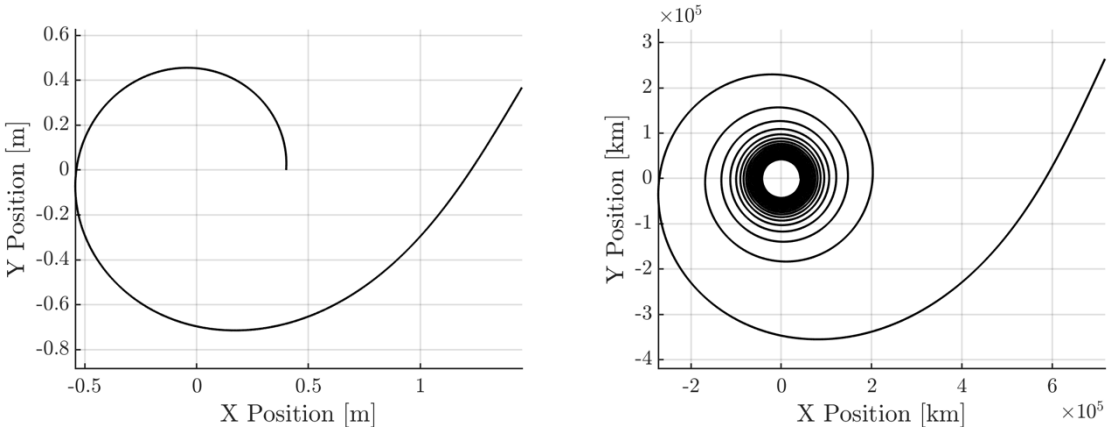

Fig. 3 Comparison of scaled trajectory used for testing on the flat floor (left) and potential escape trajectory for the HiSPEED mission (right).

waypoint. Each waypoint also has a flag that indicates if the planar air bearing is required to stop at the waypoint. If the flag is not set, then the planar air bearing is only required to move through the waypoint and has no constraints on its velocity. The total time of the trajectory can be then calculated from

$$T = \sum_{j} W[j].\tau \tag{9}$$

Given a time discretization between sample points on the trajectory, Δt, the total number of required sample points can be calculated from $N = T/\Delta t$ (where sample points range from 0 to N) and the sample point for a specific waypoint can be calculated from

$$n_j = \frac{1}{\Delta t} \sum_{i=1}^{j} W[i].\tau \tag{10}$$

It is assumed for this test that Δt and the timing between waypoints are chosen such that the calculations for N and n_j return integer values. The optimization is then

$$\min_{u} f = \sum_{i=0}^{N-1} |u_x[i]| + |u_y[i]| \tag{11}$$

where $|u_x|$ and $|u_y|$ are slack variables necessary to include the magnitude of the inputs as the cost function for the linear program. The slack variables are constrained as

$$|u_{x/y}[i]| \geq u_{x/y}[i] \tag{12}$$

and

$$|u_{x/y}[i]| \geq -u_{x/y}[i] \tag{13}$$

where $u_{x/y}$ are the input thrust along the x- and y-axes. The constraints of Eqs. 12 and 13 along with the optimization function in Eq. 11 ensure that the slack variables correspond to the actual absolute values of the input thrusts. Additional constraints include dynamics constraints

$$\begin{bmatrix} x[i+1] \\ y[i+1] \\ v_x[i+1] \\ v_y[i+1] \end{bmatrix} = \begin{bmatrix} 0 & 0 & 1 & 0 \\ 0 & 0 & 0 & 1 \\ 0 & 0 & 0 & 0 \\ 0 & 0 & 0 & 0 \end{bmatrix} \begin{bmatrix} x[i] \\ y[i] \\ v_x[i] \\ v_y[i] \end{bmatrix} + \begin{bmatrix} \Delta t^2/2 & 0 \\ 0 & \Delta t^2/2 \\ \Delta t & 0 \\ 0 & \Delta t \end{bmatrix} \begin{bmatrix} u_x[i] \\ u_y[i] \end{bmatrix} \tag{14}$$

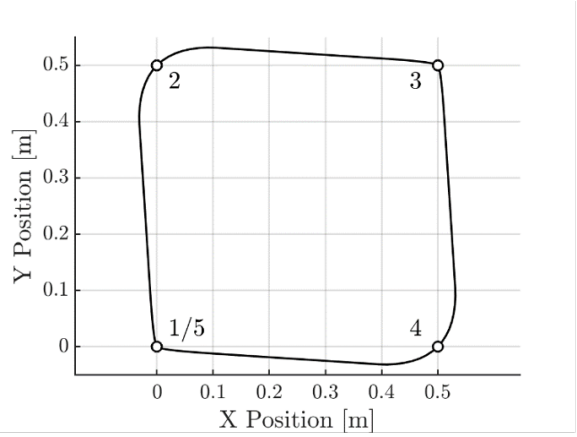

Fig. 4 Example trajectory generated with linear programming.

thrust saturation constraints

$$|u_{x/y}[i]| < u_{\max} \tag{15}$$

initial state constraints

$$\begin{bmatrix} x[0] \\ y[0] \\ v_x[0] \\ v_y[0] \end{bmatrix} = \begin{bmatrix} x_0 \\ y_0 \\ v_{x,0} \\ v_{y,0} \end{bmatrix} \tag{16}$$

and waypoint constraints

$$\begin{bmatrix} x[n_j] \\ y[n_j] \end{bmatrix} = \begin{bmatrix} W[j].x \\ W[j].y \end{bmatrix} \tag{17}$$

which includes stopping constraints for waypoints where the δ flag is set

$$\begin{bmatrix} v_x[n_j] \\ v_y[n_j] \end{bmatrix} = \begin{bmatrix} 0 \\ 0 \end{bmatrix} \qquad \text{if } W[j].\delta = 1 \tag{18}$$

For an initial implementation, velocity constraints were only included if the planar air bearing is required to stop at a given waypoint. However, velocity waypoints, where the planar air bearing is required to have a specific velocity at a given waypoint, can be easily added within this framework by replacing the right-hand-side of Eq. 18 with the desired velocity. While obstacle avoidance was not considered in this initial test, obstacle avoidance constraints can be included by using mixed-integer linear programming [17].

Figure 4 shows an example trajectory generated with the linear programming approach. The planar air bearing starts at (0, 0) and moves clockwise in a 0.5 m square. Waypoints are provided at the corners of the square and the planar air bearing has 10 s to move between each waypoint. Flags to indicate that the planar air bearing should stop are set for waypoints 3 and 5. The planar air bearing approaches and stops at waypoints 3 and 5, while for waypoints 2 and 4, the planar air bearing rounds the corner to move towards the next waypoint while minimizing control usage.

C. Spacecraft State Availability along Trajectory

To provide state feedback to the platform, the position, velocity, and orientation are updated every 10 ms. Given that the trajectory is a scaled representation of a real spacecraft trajectory, this rate would correspond to an update of the position estimate used by the onboard controller software once every 7.2 s during the mission, which is a scaled update period for receiving updates provided by the Deep Space Network (DSN). To further increase the amount of position

Table 1 Proportional and derivative control parameters for position and attitude.

Gains	Position [N/m,N/(m/s)]	Attitude [N/rad, N/(rad/s)]
Proportional	4	0.2
Derivative	10	0.5

feedback available during the mission, an optical tracking system would be used that would detect illuminated bodies and approximate the position of the satellite from the size and position of the celestial body. Using this positioning information and infrequent updates from the DSN, an accurate position estimate can be maintained at all times. If a different rate of DSN feedback is required, such as during proximity operations when a DSN position estimate may not be continuously available, the frequency of the data used by the controller can be updated, allowing the platform to simulate a wide range of mission scenarios.

In order to significantly reduce the rate of position updates that the platform receives, the onboard position estimation and position propagation must be updated. Currently, if a Vicon data packet is not received, the platform assumes a constant velocity and linearly propagates its position forward in time based on the onboard clock.

IV. Thruster Control Development

The position and attitude controllers on the platform are both Proportional-derivative (PD) controllers with gains, shown in Table 1. Through empirical tuning, the control gains were designed to be slightly overdamped. The position and attitude controllers calculate the necessary force and torque that should be exerted on the platform, which are then multiplied by a mixing matrix in order to determine the duration for which each of the eight thrusters on the platform should fire. Every ten milliseconds, the thruster controller opens the required thrusters to full for a portion of the ten millisecond time period such that the average thrust is equal to the thrust requested by the mixing matrix. If the thrust required is greater than the maximum thrust of the platform, the thruster is opened for the largest possible time period. If the thrust required is less than the minimum impulse of the thrusters, calculated by the fastest opening and closing time of the solenoid driven by the platform's computer board delays, the platform will not open the thruster at all, preferring to undershoot rather than overshoot, possibly inducing oscillation and instability. This overall process cannot perfectly represent a continuous thrust system, possibly introducing resultant thrust direction errors that are treated as disturbances for the controller.

Integral control could be beneficial during trajectory following operations to reduce errors that last on the order of tens of seconds to the limits of the propulsion system's minimum impulse capabilities. In many of the tested trajectories, the platform exhibits position errors persisting for tens of seconds, an issue that should be remedied with properly tuned integral control. However, because of the minimum impulse of the thrusters, it was observed that integral error would build up over time and eventually cause the platform to oscillate within the thruster deadband. Consequently, the testing described in the next section uses only proportional-derivative control. The HiSPEED concept, with its continuous thrust actuators, would not exhibit this behavior.

V. Hardware Testing

A. Design of Experiments and Test Setup

All experiments done on the test platform were performed on the leveled granite table in the SSDT or on the FCT flat floor. If the platform needed to move for testing a trajectory or controller, the FCT flat floor was used. If only stationary testing was required, the granite table in the SSDT was used because of the small size of the granite table. For tests in the FCT, the command to start the test was sent to the platform from the ground station after all human operators were clear of the Vicon system line-of-sight to the platform.

Once a trajectory was completed, a log file recording the position, velocity, thruster commands, and ground station communication status can be downloaded from the Atlas. A similar log file with the same position and velocity data can also be downloaded from the Vicon system if communications between the platform and ground station were either accidentally or intentionally interrupted. A list of messages from the Atlas computer can also be obtained, which shows

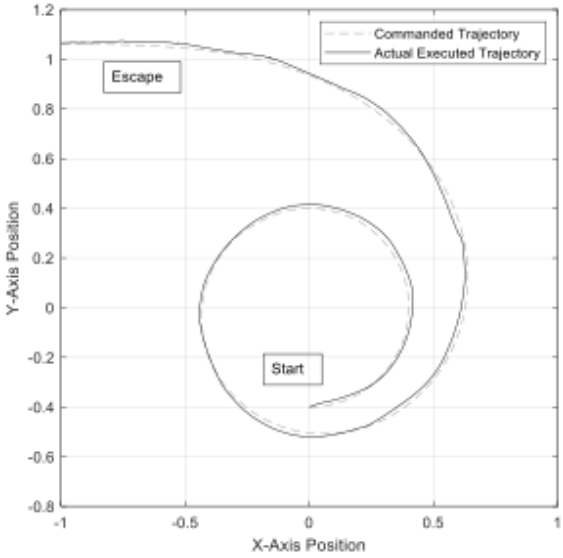

Fig. 5 Escape spiral starting from geostationary orbit.

any potential errors or other program messages.

B. Summary of Test Results

In its current capacity, the platform is capable of following a variety of model trajectories. One such trajectory that was tested extensively on the FCT flat floor was the scaled prograde-facing escape spiral discussed previously in this paper. The platform started 40 cm from the center of the spiral in the negative y-direction and move in a counterclockwise spiral while maintaining a prograde direction. This trajectory is very similar, though scaled, to an escape trajectory by the 15 kg HiSPEED spacecraft, using an electrospray thruster system with approximately 5.1 mN of thrust. The trajectory starts near a geosynchronous orbit due to physical constraints of the platform and ends with a representative escape to rendezvous with an asteroid after escape. The platform uses its thrusters to both simulate the pull of gravity and the force of the thrusters to slowly raise its orbit to escape. The trajectory the platform followed during tests is displayed in Fig. 5.

The performance of the platform during this escape trajectory is representative of what could be expected from the platform while running arbitrary trajectories with feedforward thrust. For this trajectory, the feedforward thrust never exceeded 0.2 N, or 20% of the platform's maximum thrust, as each thruster can produce approximately 0.5 N on its own, allowing for 1 N of thrust in any given direction. Having lower levels of feedforward thrust and moving slower on the floor allows the platform to perform more accurately as the controller can respond to a growing position error before the error grows to the level at which the platform must move near its maximum speed to execute the closed loop control.

The trajectory starts with an initial state and velocity, however because the vehicle starts from rest, there is a large initial error at the start of the trajectory as the vehicle accelerates to match the commanded trajectory. On the first step of the trajectory, the platform senses the initial error in required speed and quickly accelerates. The first few moments of each trajectory, therefore, exhibit higher velocity errors and a growing position errors due to this velocity difference. Consequently, relatively high force is commanded. The effect on the trajectory is that of a slight deviation from the ideal path. When the platform begins to lag behind the target state, the platform undershoots the desired spiral in an attempt to catch up to the outwardly-growing reference trajectory. This effect can be seen near the "Start" point in Fig. 5, where the position of the platform is noticeably inside that of the trajectory as well as in the velocity and position error plots in Fig. 6.

For the majority of the trajectory, the position error stays within ±4 cm of the target position. The two horizontal lines on Fig. 6 are representative of the "dead zone" of the platform. Because of the inherent delays in the driver of controlling computer, the minimum thrust of any thruster is 0.1 N: the 40 ms delay in the Emerald when opening a solenoid is 20% of the 200 ms period on which the thrusters are opened. Therefore, if a thruster is opened, it is open for at least 40 ms at 0.5 N of thrust. The platform will not open a thruster unless the burn duration requested is larger

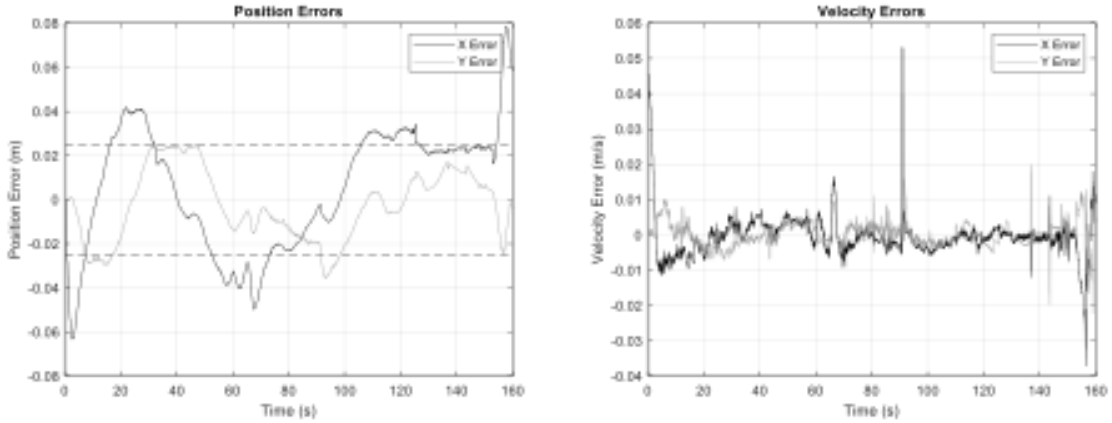

Fig. 6 Position and velocity error over time during escape trajectory maneuver.

than the 40 ms limit, so the smallest position error which will result in the platform opening a thruster is 2.5 cm: for a lesser amount, the required impulse to correct would be smaller than the minimum impulse of the platform and any correction would most likely result in significant overshoot. The only major exceedances are at the beginning and end of the trajectory. Notably, the error spike at the end of the trajectory is due to an aggressive rotation maneuver for the purposes of demonstrating basic proximity operations capabilities entirely separate from the escape trajectory. The rotation that caused the large position error spike was a 180 degree rotation step, creating high angular error and therefore causing the platform to react with large thrust commands. For this system, as the commanded translation or rotation rate increases, the ability of the platform to control other degrees of freedom decreases owing to a thrust scaling effect in the controller. When the controller calculates which thrusters fire and the corresponding firing duration, it commands the sum of the forces and torques calculated by the position controller and the attitude controller, either of which can individually command a thrust that exceeds the maximum impulse of the thrusters. Consequently, the resultant thrust can be dominated by the need to correct for a high rotational error, masking the contribution to the net thrust for small position errors. The inverse problem is also observable in which large position errors generate thrust commands significantly larger than thrust commands to counter small attitude errors. Therefore, with a limited force that can be generated per thruster, a controller cannot meet the demands of simultaneous high translation and rotation commands. The gain and phase margins set by the system bandwidth therefore determine the point at which instability will result.

The velocity plot in Fig. 6 is similar to the position error in that there is a minimum velocity error that will produce a thrust. With a minimum thrust of 0.1 N and a translational derivative gain of 10 N/(m/s), the platform can have up to a 1 cm/s error in its velocity before the platform will burn to correct it, assuming that it is positioned perfectly. From Fig. 6, the velocity stays well within this band, only deviating at the beginning and at data spikes in the middle and at the end of the test run. Information about the angular velocity of the platform is also computed on the Vicon system and suffers from the same effects.

The attitude controller, like the position controller, uses PD control to hold the heading of the test platform to where the trajectory file states it should be. Like the position controller, it utilizes state error to augment a feedforward torque to pass to the thruster controller. The test platform does not perform the calculations that transform position data into velocity data, so the spikes in velocity result from variability in the Vicon system. The Vicon has several issues that might cause data artifacts like those in Fig. 6: loss of line of sight from one or more tracking objects, obscuration of tracking cameras, and loss of signal from the Vicon system to the platform.

C. Position Tracking Performance on Air Bearing

The platform is tracked with six tracking objects placed in various locations on the hardware. Four of the objects are above the top plate, mounted either on standoffs or on top of stationary components mounted to the plate. These objects should be in view at all times, regardless of rotation. Two of the objects, added to increase the accuracy of the Vicon, are mounted on the sides of the platform and will therefore shift in and out of the field of view of any individual camera depending on the orientation of the platform. As it moves across the floor, the platform also drifts into and out of the

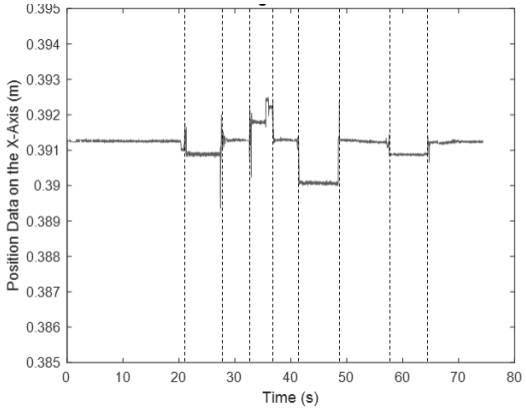

Fig. 7 Vicon position data with tracking balls incrementally covered; vertical lines indicate times when target objects were obscured.

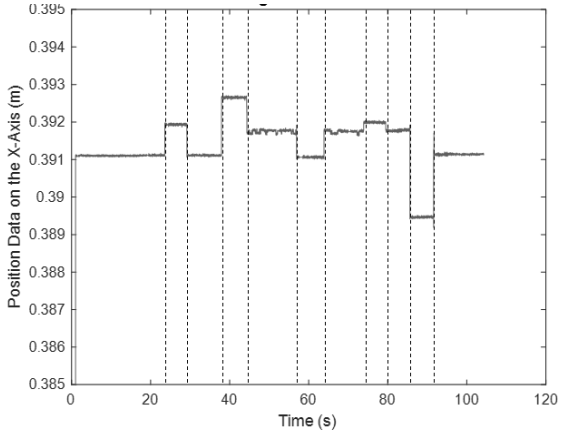

Fig. 8 Vicon position data with cameras incrementally covered; vertical lines indicate times when cameras were obscured.

field of view of certain cameras, which cannot view the entire floor at one time. Any interruption of vision between a camera and a tracking object may result in position discontinuities. Although the velocity data is filtered, these position discontinuities help explain why artifacts appear in the velocity data.

On the prototype test platform without thrusters in the SSDT Lab, four tracking objects are viewed by five cameras, positioned evenly around the object. To test the magnitude of the position discontinuities, each object was covered and then uncovered by an opaque plastic cup so that none of the cameras would be able to see the target object. Care was taken not to accidentally obscure vision of any of the other target objects while one was being covered. After a few seconds, the target was uncovered and the process repeated with the other cups mounted on the prototype platform. The data log, generated by the Vicon system and stored on the ground station, was then plotted in Fig. 7 to reveal discontinuities of up to 3 mm across the highest and lowest point. With the Vicon running at its maximum rate of 100 samples per second, a 3 mm position discontinuity would result in a 0.3 m/s velocity spike, a significant jump for a platform traveling at no more than 0.1 m/s in normal operation. Such results play a key role in assessing controller performance, and tests using similar truth sensor systems must account for such behaviors.

The Vicon obscuration test was then repeated, but instead of covering individual tracking objects, individual cameras were obscured by a large plastic sheet (a deterministic method for this test as opposed to stochastic effects such as personnel moving in the test volume), such that the covered camera had no line of sight to any of the tracking objects, but all other cameras still had clear line of sight to all four tracking objects. This was repeated for each camera around the room. When plotted in Fig. 8, the discontinuities found while covering individual tracking objects are still present, with peak-to-peak amplitude of over 4 mm, leading to a theoretical 0.4 m/s velocity spike.

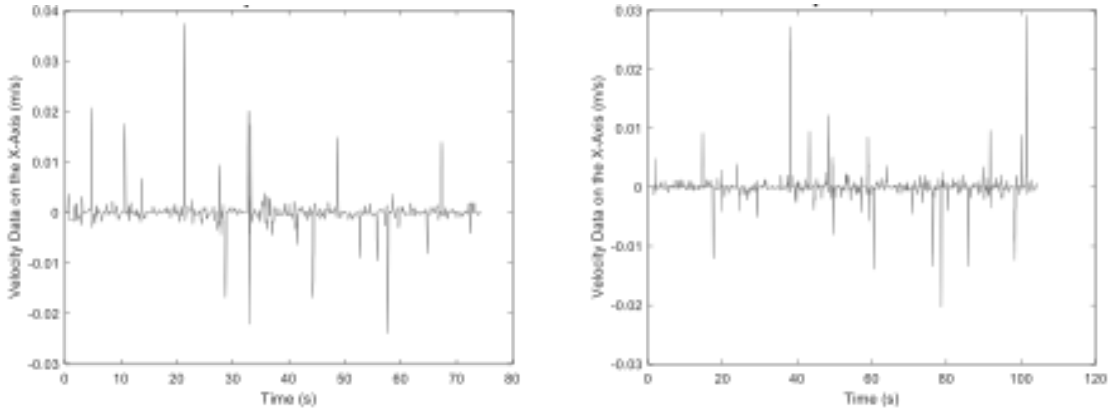

Fig. 9 Vicon velocity data with tracking balls (left) and cameras (right) incrementally covered.

When transformed into velocity data, position data is first passed through a 30th order finite impulse response filter, which still is not able to remove the velocity spikes completely from the data fed to the test platform. The same data used in Fig. 7 and Fig. 8 was passed through the filter and the exact velocity data that would be passed to the platform during a test was recorded. Although no velocity spikes over the theorized 0.4 m/s were observed, many prominent spikes lining up with the discontinuities in the position data litter Fig. 9, anywhere from 0.5 cm/s to almost 4 cm/s, about as large as the velocity spikes observed in the actual velocity error data taken from the real test run on the FCT flat floor.

Steps to ameliorate velocity errors such as these can easily be taken. Increasing the number of cameras on the floor increases tracking reliability and reduces the magnitude of errors seen in velocity data. An even easier way to reduce measurement error is to attach more tracking objects to the platform in more visible locations. Objects placed above the highest point on the platform are ideal as they are least likely to be obscured as the platform translates and rotates. Objects below the highest point of the platform would ideally be removed, as they are guaranteed to be blocked from one or more cameras at certain headings. To avoid certain errors where the Vicon cannot determine the exact state of an object due to ambiguous orientation states, the objects should form a clearly three-dimensional object.

Upcoming simulation developments are focusing on the prediction of flight performance, using models of the HiSPEED thruster configuration, an approximation of a flight vehicle's mass properties, and the full, un-scaled trajectory. These simulations build upon the testing discussed in this paper. The tests provide valuable insight into flight performance that will not be affected by the gravity limitations that reduce testing degrees of freedom or the environmental disturbances encountered as a result of operating on a planar air bearing. Importantly, the testing of the newly-developed small satellite planar air bearing thruster system provides guidance as to how controllers should be developed for low thrust missions like HiSPEED based on the availability of truth data to position and attitude estimators, deadband limitations on thruster controllers, and necessary computational and thruster architectures to maintain controllability throughout the mission.

VI. Conclusions

A. Summary of Current State

The developments presented in this paper show the ability of the Small Satellite Dynamics Testbed to conduct spacecraft dynamics testing using a newly-developed thruster system, with the HiSPEED project as an example. The thrusters onboard the planar air bearing platform have been used to demonstrate a trajectory-following controller that was developed for the HiSPEED mission. Additionally, the trajectory used for the demonstration testing was a scaled version of the actual planned trajectory to a near-Earth asteroid. While following the scaled trajectory, the system remained within ±4 cm of the commanded trajectory while commanding compressed air thrusters instead of the HiSPEED mission's electrospray thrusters, which provide more granular firings. Although these 4 cm errors translate to errors on the order of 105 km in the HiSPEED trajectory, this error is caused by a combination of limitations in the state knowledge from the Vicon system and the limited number of thrust levels possible with the compressed air thrusters. Future tests in simulation will work towards determining a proper relationship between errors observed on the flat floor

and those expected on the actual HiSPEED system. By conducting this testing, the HiSPEED mission concept has gained an invaluable tool for developing controllers that can maintain pointing along a prescribed trajectory and for maturing hardware components needed for implementing the staged electrospray system that is unique to HiSPEED. The analysis of the errors and uncertainty bounds in testbed data provides metrics for assessing the performance of both hardware and software for HiSPEED, with extensibility to other future missions.

B. Planned Future Updates

Although the system can track to given trajectories within several centimeters of error, the capabilities of the platform could be augmented to increase both the accuracy of position tracking and add additional functionality. One of the most beneficial optimizations to the platform would be the reduction of the minimum impulse of the thrusters, allowing for more precise movement. Adjustments to the structure of the PD controller could reduce the dead band in the controller, leading to reduced steady-state error and increased trajectory accuracy. Coupled with the lower minimum-impulse bit, gain scheduling could allow the platform to compensate the effects of static and kinetic friction, making the lower minimum impulse more effective. Lessons learned from this process would impact how controllers for flight are tuned, especially because flight hardware would not need to cope with the need to compensate for disturbances created by operating in the ground environment. Hardware could also be added to mimic the behavior of thruster staging, of particular use to the HiSPEED program, where adjustments to the attitude control systems of the spacecraft must be made to account for the shifting center of mass and adjusted rotational moments of inertia at staging events. To further mimic the flight conditions of the HiSPEED mission, the rate at which the platform receives data could be reduced so that the platform would rely more on its internal estimation of its position rather than the frequent updates from the Vicon system.

The current Emerald board that controls the opening of the thrusters has a significant 36.5 ms delay built into its driver. This delay occurs twice whenever a thruster is turned on; once to raise the pin and open the thruster, and once to lower the pin and allow the thruster to be turned off by the Atlas board. Effectively, the thrusters have a minimum open time of 40 ms, as the flight software is frozen while the Emerald board delay occurs, which translates to a 0.1 N minimum thrust, or a 0.02 Ns impulse. Although lowering the Emerald delay by updating the driver is possible, the SSDT currently plans to upgrade the hardware to a Sphinx board so that the platform will operate using flight-equivalent hardware and software for computation and command and data handling, which would presumably remove the delay, as it is unlikely that a different computer made by a different manufacturer would share this unusual characteristic. With the current controller timing, removing the delay upon opening thrusters would reduce the theoretical minimum thruster open time to 10 ms, resulting in a 0.025 N minimum thrust or 0.005 Ns minimum impulse.

Reducing the minimum impulse was previously not considered a high priority because the current minimum impulse of the platform is not enough to overcome static friction with the floor. Although the air bearing platform is supposed to not be in contact with the floor at all, due to irregularities and deformities in the testing floor, certain areas of the floor have more friction than others and during position hold tests, the platform was observed firing a single thruster for the minimum duration and not reaching steady state. A minimum impulse is desired to prevent the platform from wasting air unnecessarily, as if the platform does not generate enough thrust to overcome friction, it will not move and continue to waste air. While the platform is moving, however, the dynamic friction between the floor and the platform is lower than that between the stationary platform and the floor, meaning that the desired minimum impulse while moving is significantly smaller than the desired minimum impulse while stationary. Artificially setting a minimum impulse depending on whether the platform is moving or stationary would effectively allow the controller to compensate for the difference in performance and benefit from the augmented performance of a lower minimum impulse while not wasting fuel making small burns in a position hold mode.

VII. Funding Sources

Financial support for the work presented in this paper comes from the NASA Small Satellite Technology Program (SSTP) through grants 80NSSC18M0045 and 80NM0018D0004, and the NASA Space Technology Research Fellowship (NSTRF) program through grant 80NSSC18K1186.

VIII. Acknowledgements

Financial support for the work presented in this paper comes from the NASA Small Satellite Technology Program (SSTP) through Grants 80NSSC18M0045 and 80NM0018D0004, and the NASA Space Technology Research Fellowship (NSTRF) program through Grant 80NSSC18K1186. The authors would like to acknowledge the assistance of Carl Seubert for his management and oversight of the Jet Propulsion Laboratory (JPL) Formation Control Testbed and John Ziemer for his role as NSTRF mentor for Oliver Jia-Richards. The research was carried out at JPL, California Institute of Technology.

References

[1] Chin, A., Coelho, R., Nugent, R., Munakata, R., and Puig-Suari, J., "CubeSat: The Pico-Satellite Standard for Research and Education," *Proceedings of the AIAA SPACE Conference & Exposition*, American Institute of Aeronautics and Astronautics, San Diego, California, USA, 2008. https://doi.org/10.2514/6.2008-7734.

[2] Sternberg, D., Essmiller, J., Colley, C., Klesh, A., and Krajewski, J., "Attitude Control System for the Mars Cube One Spacecraft," *Proceedings of the IEEE Aerospace Conference*, Institute of Electrical and Electronics Engineers, Big Sky, Montana, USA, 2019. https://doi.org/10.1109/AERO.2019.8741816.

[3] Smith, C., Cheek, N., Burnside, C., Baker, J., Adell, P., Picha, F., Kowalkowski, M., and Lightsey, E., "The Journey of the Lunar Flashlight Propulsion System from Launch through End of Mission," *Proceedings of the Small Satellite Conference*, Utah State University, Logan, Utah, USA, 2023.

[4] Krejci, D., Gomez Jenkins, M., and Lozano, P., "Staging of Electric Propulsion Systems: Enabling an Interplanetary CubeSat," *Acta Astronautica*, Vol. 160, 2019, pp. 175–182. https://doi.org/10.1016/j.actaastro.2019.04.031.

[5] Jia-Richards, O., Sternberg, D., Grebow, D., Mohan, S., and Lozano, P., "Feasibility of a Deep-Space CubeSat Mission with a Stage-Based Electrospray Propulsion System," *Proceedings of the IEEE Aerospace Conference*, Institute of Electrical and Electronics Engineers, Big Sky, Montana, USA, 2020. https://doi.org/10.1109/AERO47225.2020.9172544.

[6] Jia-Richards, O. and Lozano, P., "Stage-Based Electrospray Propulsion System for Deep-Space Exploration with CubeSats," *Proceedings of the IEEE Aerospace Conference*, Institute of Electrical and Electronics Engineers, Big Sky, Montana, USA, 2019. https://doi.org/10.1109/AERO.2019.8742094.

[7] Jia-Richards, O. and Lozano, P., "Laboratory Demonstration of a Staging System for Electrospray Thrusters," *Proceedings of the International Electric Propulsion Conference*, Electric Rocket Propulsion Society, Vienna, Austria, 2019.

[8] Sternberg, D., Pong, C., Filipe, N., Mohan, S., Johnson, S., and Jones-Wilson, L., "Jet Propulsion Laboratory Small Satellite Dynamics Testbed Simulation: On-Orbit Performance Model Validation," *Journal of Spacecraft and Rockets*, Vol. 55, No. 2, 2018, pp. 322–334. https://doi.org/10.2514/1.A33806.

[9] Wapman, J., Sternberg, D., Lo, K., Wang, M., Jones-Wilson, L., and Mohan, S., "Jet Propulsion Laboratory Small Satellite Dynamics Testbed Planar Air-Bearing Propulsion System Characterization," *Journal of Spacecraft and Rockets*, Vol. 58, No. 4, 2021, pp. 954–971. https://doi.org/10.2514/1.A34857.

[10] García Yárnoz, D., Sanchez, J. P., and McInnes, C. R., "Easily Retrievable Objects among the NEO Population," *Celestial Mechanics and Dynamical Astronomy*, Vol. 116, 2013, pp. 367–388. https://doi.org/10.1007/s10569-013-9495-6.

[11] Vanelli, C., Swenka, E., and Smith, B., "Verification of Pointing Constraints for the Dawn Spacecraft," *Proceedings of the AIAA/AAS Astrodynamics Specialist Conference*, American Institute of Aeronautics and Astronautics, Honolulu, Hawaii, USA, 2008. https://doi.org/10.2514/6.2008-7085.

[12] Kennedy, B., Abrahamson, M., Ardito, A., Han, D., Haw, R., Mastrodemos, N., Nandi, S., Park, R., Rush, B., and Vaughan, A., "Dawn Orbit Determination Team: Trajectory and Gravity Prediction Performance During Vesta Science Phases," *Proceedings of the AAS/AIAA Space Flight Mechanics Meeting*, American Astronautical Society, Kauai, Hawaii, USA, 2013.

[13] Whiffen, G., "Mystic: Implementation of the Static Dynamic Optimal Control Algorithm for High-Fidelity, Low-Thrust Trajectory Design," *Proceedings of the AIAA/AAS Astrodynamics Specialist Conference*, American Institute of Aeronautics and Astronautics, Keystone, Colorado, USA, 2006. https://doi.org/10.2514/6.2006-6741.

[14] Rayman, M. D., Chadbourne, P. A., Culwell, J. S., and Williams, S. N., "Mission Design for Deep Space 1: A Low-Thrust Technology Validation Mission," *Acta Astronautica*, Vol. 45, No. 4–9, 1999, pp. 381–388. https://doi.org/10.1016/S0094-5765(99)00157-5.

[15] Jia-Richards, O. and Lozano, P., "Analytical Guidance for Circular Orbit Transfers with Staging of Electrospray Propulsion Systems," *Acta Astronautica*, Vol. 179, 2021, pp. 69–77. https://doi.org/10.1016/j.actaastro.2020.10.034.

[16] Tillerson, M., Inalhan, G., and How, J., "Co-ordination and Control of Distributed Spaeccraft Systems Using Convex Optimization Technique," *International Journal of Robust and Nonlinear Control*, Vol. 12, No. 2–3, 2002, pp. 207–242. https://doi.org/10.1002/rnc.683.

[17] Richards, A., Schouwenaars, T., How, J., and Feron, E., "Spacecraft Trajectory Planning with Avoidance Constraints Using Mixed-Integer Linear Programming," *Journal of Guidance, Control, and Dynamics*, Vol. 25, No. 4, 2002, pp. 755–764. https://doi.org/10.2514/2.4943.